Tunable Quantum Dot Arrays by Self-Assembled Metal-Organic Networks

F. Klappenberger,[1,*] D. Kühne,[1] W. Krenner,[1] I. Silanes,[2,3] A. Arnau,[2,4,5]
F. J. García de Abajo,[6] S. Klyatskaya,[7,1] M. Ruben,[7,8] and J. V. Barth[1]

[1]*Physik Department E20, TU München, 85748 Garching, Germany*

[2]*Donostia International Physics Center (DIPC), 20018 San Sebastian, Spain*

[3]*Instituto de Hidráulica Ambiental de Cantabria (IH), 39005 Santander, Spain*

[4]*Centro de Fisica de Materiales CSIC-UPV/EHU,*
Materials Physics Center MPC, 20080 San Sebastian, Spain

[5]*Depto. Fisica de Materiales UPV/EHU, Facultad de Quimica, 20080 San Sebastian, Spain*

[6]*Instituto de Óptica – CSIC, Serrano 121, 28006 Madrid, Spain*

[7]*Institute für Nanotechnologie, Karlsruher Institut für*
Technologie (KIT), 76344 Eggenstein-Leopoldshafen, Germany

[8]*IPCMS-CNRS, Université de Strasbourg, F-67034 Strasbourg, France*

(Dated: December 6, 2010)

The confinement of Ag(111) surface state electrons by self-assembled, nanoporous metal-organic networks is studied using low-temperature scanning tunneling microscopy/spectroscopy and electronic structure calculations. The honeycomb networks of Co ligands and dicarbonitrile-oligophenyl linkers induce surface resonance states confined in the cavities with a tunable energy level alignment. We find that electron scattering on the molecules is repulsive and stronger than on the weakly attractive Co and that the networks represent periodic arrays of coupled quantum dots featuring uniform electronic levels.

The controlled adjustment of materials properties by modification on the atomic scale is a major goal of nanoscale science. On the close-packed faces of noble metals the surface state electrons are well suited to monitor and influence the properties of the surface [1]. In 1993 Crommie *et al.* demonstrated the engineering of quantum well states by the manipulation of individual adatoms [2]. Since then the quasiparticle excitations of the surface state band have been studied with great interest both experimentally [3–8] and theoretically [9–12],

especially because their lifetime is connected to elementary scattering processes [10, 11]. The high level of control over local electronic properties achievable by atom manipulation was demonstrated in the quantum mirage effect [13], in the controlled modification of the electronic structure of an adsorbate[14], or in quantum holographic encoding [15].

However, for the design of a targeted electronic spectrum of an *entire* surface it is impractical to use atom manipulation due to the slow serial production process. Since not only metal adatoms but also organic molecules scatter the surface state electron waves [16], the extended regular structures that can be produced with molecular self-assembly [17] allow the tuning of electronic properties not only locally but surface wide, for example in between linear molecular lines [18]. An elaborate electronic structure has been bestowed to Ag(111) by a chiral Kagomé network providing a 2D periodic array of quantum dots [19]. With the reflectivity for the electron waves being finite, the leakage-induced electronic overlap between neighboring quantum dots results in dispersive bands [20].

Here, we use supra-molecular design to construct metal-organic networks providing regular hexagonal cavities on the Ag(111) metal surface [21, 22]. The obtained room-temperature stable, nanoporous arrays create a novel periodic structure to the surface state electrons in which the energy positions of the different resonances depend on the lateral dimensions of the confinement region. These dimensions are easily tunable by the length of the linking molecule. The electronic characteristics of the confined states have been reproduced both in energy and real space by Green's functions based electronic structure calculations using a boundary element method. Our analysis indicates that the molecules produce a repulsive scattering potential whereas the Co ligand potential is slightly attractive. Thus the coordination bond markedly alters the scattering properties of the Co atoms. The crystal-like quality of our networks provides a perfect template for the lateral engineering of surface states [23] as well as for the production of surface plasmon polariton waveguides [24].

The experiments were carried out in a vacuum apparatus with a base pressure of $\sim 3 \times 10^{-11}$ mbar, where a clean Ag(111) surface was prepared by repeated cycles of Ar^+ sputtering and annealing to 740 K. Dicarbonitrile-quaterphenyl (NC-Ph_4-CN) and dicarbonitrile-sexiphenyl (NC-Ph_6-CN) molecules [21, 22] were sublimated from a quartz glass crucible inside a Knudsen cell, held at 483 K for NC-Ph_4-CN and at 572 K for NC-Ph_6-CN, onto the Ag substrate stabilized at room temperature (RT). The deposition time for a dense-packed monolayer [25] is approximately 10 mins. After the sublimation of the

organic molecules, Co adatoms were dosed by e-beam evaporation while keeping the substrate at RT. Posteriorly, the sample was transfered into our home-made [26] beetle-type low-temperature STM where data were recorded at $\approx$ 8 K. The indicated bias values V_{B} refer to the sample voltage. Scanning tunneling spectroscopy (STS) was carried out by open-feedback loop dI/dV point spectra with set points as indicated, bias modulation with frequencies $\sim$1400 Hz, an amplitude of 5 mV rms, and a lock-in time constant of 20 to 50 ms. The dI/dV maps were extracted from a set of 84 x 84 point spectra equally distributed over the area of interest. All spectra were normalized such that the average value of the intensity between -250 mV and -150 mV was 1. The spectroscopic maps are displayed as measured *without* convolution or high pass filtering. The automated procedure for taking a set of spectra takes 10 to 20 h, therefore maps are slightly distorted due to drift.

We reported previously [22] that after the evaporation of 3 parts NC-Ph_6-CN and 2 parts Co [Fig. 1(a)] large domains of RT stable metal-organic networks self-assemble as exemplified in Fig. 1(b). These supramolecular structures provide regular arrays of uniform hexagonal pores. The spectroscopic dI/dV map obtained at a bias value $V_{\mathrm{B}} = 101$ mV [Fig. 1(c)] demonstrates a standing electron wave pattern indicating confinement [2, 3, 8, 19, 27] of the electrons of the surface state described by the energy dispersion $E(k) = E_0 + \frac{\hbar^2}{2m^*}k^2$, where $E_0 = -65$ meV is the onset energy, $m^* = 0.42m_e$ the effective mass [27, 28], $\hbar$ the reduced Planck constant, and k the electron wave vector. Thus, each pore represents a quantum dot. Earlier work showed that for this network type the size of the unit cell is controlled by the length of the organic linker [21]. As a consequence, the confinement imposed by the networks can be tuned accordingly. As an example we chose NC-Ph_4-CN [Fig. 1(d)] to construct quantum dots with a reduced confinement area [Fig. 1(e)]. Now, the same standing wave pattern is obtained at a higher $V_{\mathrm{B}} = 204$ mV. In comparison to confinement in previous, sputtered or grown, nanostructures [4, 7, 8, 29] the intensity distributions of the network-confined resonances exhibit more regular shapes directly reflecting the hexagonal symmetry of the networks. Furthermore, the identical spectroscopic features in the different pores [Figs. 1(c) and (f)] reveal the crystal-like quality that can be achieved by using self-assembly protocols for the production of such arrays of quantum dots.

For a more quantitative investigation of the confinement properties, we focus on the NC-Ph_6-CN case in the following, before discussing the tunability in more detail later. A set of representative points of the hexagonal unit cell [Fig. 2(a)] was chosen to conduct dI/dV

point spectroscopy [Fig. 2(b)]. In contrast to the reference spectrum (gray dashed line), recorded over a pristine surface with the same tip that was used to obtain all the spectra of the set, a strong position dependent variation is present in the spectra distributed over the quantum dot. The *c*-spectrum (black, plus symbols), i.e., the spectrum at the center of the hexagon, shows two clear maxima at $V_{\mathrm{B}} = -6$ and 205 mV, with the second maximum being enclosed by a shoulder on the low as well as on the high energy side ($V_{\mathrm{B}} \approx 140$ and 280 mV). The *h*-spectrum (red, crosses), obtained at half of the distance between the center of the cavity and the center of a molecule, displays its most prominent peak at 68 mV. The *mol*-spectrum (blue squares), on top of the center of a molecule, indicates the smallest local density of states (LDOS) of all positions and appears without sharp features. The *Co*-spectrum (green diamonds), on top of a single coordinated Co ligand, shows more intensity than the *mol*-spectrum for $V_{\mathrm{B}} < 150$ mV, and very similar intensity for higher bias values. Therefore, the difference between the *Co*- and the *mol*-spectrum is a first indication that, with respect to the electron scattering close to the Fermi level, the two positions behave differently.

In the following we will analyze our system in a first approximation by comparing it to a quantum particle in a 2D hexagonal box [29]. The lowest eigenstates Ψ_n of this system that exhibit intensity in the center of the hexagon are Ψ_1 and Ψ_4. They are reflected in the two maxima of the *c*-spectrum in Fig. 2(b), whereas the maximum of the *h*-spectrum is connected to Ψ_2. The numerically obtained eigenvalues λ_n for the hexagonal box [29] scale with the inverse of the area of the hexagon $A = \cos\left(\frac{\pi}{6}\right) D^2$ and thus the eigenstate energies E_n for our system can be calculated by $E_n = E_0 + \frac{\lambda_n}{m^* A}$. For the 20x20 supercell obtained in ref. [22] the distance between parallel hexagon sides amounts to $D = 57.78$ Å. With this D the energy values E_n deviate from the experimental ones (Supporting information (SI), Table I). However, by using an effective diameter $D_{eff} = 1.05D$ good agreement is obtained. This indicates a substantial penetration of the wave functions into the confining potential, i.e., an appreciable overlap between neighboring quantum dots. The origin of this overlap will be further discussed after the presentation of our theoretical analysis.

Next, we investigate the lateral intensity distributions of the confined resonances. The Ψ_1 state [Fig. 3(a)] exhibits a dome-like structure inside the cavity. The molecules appear dark, the Co atoms at the coordination sites show medium brightness. A central depression surrounded by a bright ring leads to a donut shape for Ψ_2 [Fig. 3(b)]. In this case also the

corners exhibit a higher electron density than the molecules. At 200 mV [Fig. 3(c)], the map is characterized by a protrusion in the center encompassed with a dark inner and a brighter outer ring. At the energy of the 5th eigenstate [Fig. 3(d)] the central maximum is very shallow and the outer ring is divided into six bright spots near to the centers of the molecules. The comparison with the theoretical state densities of ref. [4] allows extracting two conclusions. First, the intensity in the outer ring of the Ψ_4 maps is too high compared to the central peak, but can well be explained if a mixing with Ψ_3 is taken into account. Thus the map at 200 mV is not an eigenmode but a mixture with the 3rd state that should appear at $V_{\mathrm{B}} = 174$ mV (see SI), but is not resolved because of the width of the resonances. Second, for $n = 2$ to 5, all eigenstates are expected to display maxima inside the cavity near the corners. Since the experimental maps do not show these maxima, the scattering potential of the Co atoms must be less reflective than that of the molecules.

We have gained further insight into the electron confinement properties of the network through model simulations using a scalar version of the electromagnetic Boundary Element Method (BEM) [19, 23, 30]. The Schrödinger equation is solved for a 2D potential landscape, which consists of regions of constant potential with abrupt boundaries. The solution is expressed in terms of auxiliary boundary sources, which are propagated in each region via the electron Green's function. The auxiliary sources are then determined from the continuity of both the wave function and its gradient, thus defining a system of integral equations that we solve using standard numerical techniques.

Using the already mentioned values for E_0 and m^* for the surface-state electron band, we have defined the effective scattering potential landscape as depicted in Fig. 2(c), where the black regions have zero potential and in which the molecules are described by rectangles (white) with the same length (2.96 nm), width (0.25 nm, C-C distance perpendicular to the long molecular axis), and effective scattering potential value ($V_{\mathrm{mol}} = 500$ meV) that were successfully employed earlier [19]. The value $V_{Co} = -50$ meV for the hexagonal Co regions (green) and the energy-independent phenomenological broadening (25 meV) were adjusted to obtain the best agreement with experiment.

Using the BEM, we calculated the energy dependent LDOS at selected (x,y) positions and compared them to the measured dI/dV spectra. Despite the simplicity of the model, the simulated spectra [Fig. 2(d)] agree rather well with the measured dI/dV point spectra [Fig. 2(b)] regarding peak positions, intensities and width. The only exception is the Co-

spectrum, which deviates from the experiment for $E \gtrsim 100$ meV.

Furthermore, conductance maps [LDOS(x,y)] of the resonances Ψ_i [Fig. 3(e)-(h)] were calculated at the energies E_i indicated by the maxima in the dI/dV spectra shown in Fig. 2(d). In this model description, the surface state electrons are restricted to a 2D plane and, therefore, there is not any z-coordinate representing the height. Thus, we compare with experimental spectroscopic data taken under open feedback-loop conditions, corresponding to constant height conditions. Note that all simulated maps are displayed using an identical color scale, and that the same is true for the experimental maps. Close examination of the simulated standing-wave patterns reveals a reproduction of the experimental data in great detail within the cavities. For the Co sites, the agreement is very good for energies $E < 100$ meV, but too much intensity is present at higher energies in the simulated maps, as anticipated from the dI/dV point spectra. The approximation of describing the actual three-dimensional scattering of surface state electrons by an energy independent 2D effective scattering potential has some limitations and, therefore, one cannot expect a fully correct description of the real system.

The overall agreement between the measured and the simulated shapes of the resonances substantiates that the difference between the eigenstates of a purely hexagonal quantum box and our system originates from the attractive scattering potential around the Co atoms. In contrast, an isolated Co adatom on the Ag(111) surface is characterized by an effective repulsive scattering potential for electrons at the Fermi level [31]. Thus, our study indicates that the formation of the metal-organic coordination results in a significant change of the interaction of the embedded Co centers with the surface state electrons. Even though in an extended system it is not trivial to assign a specific charge to an individual entity, we interpret this result using the following picture. The electron charge transfer from the Co centers to the CN-ligands changes the character of the electron-Co interaction from repulsive (isolated Co adatom) to attractive (Co bond to CN-ligands) for electron scattering close to the Fermi level. However, the HOMO-LUMO gap of the molecules represents a repulsive potential for these electrons, even after the formation of the metal-organic coordination.

Now we discuss the tunability of the energetic positions of the quantum dot states in more detail. In Fig. 4 we compare the c-spectra of the networks constructed from NC-Ph_6-CN and NC-Ph_4-CN. The characteristic features (highlighted by vertical lines) shift to higher energies for the shorter molecules. As shown in the SI, we obtain a constant scaling ratio

$R_{exp} = 1.74$ for all four features marked in the Figure proving that the energy levels are controlled by the quantum dot dimensions. A version of the NC-Ph_4-CN-spectrum with the bias values scaled by R_{exp} highlights that the shape of the spectrum remains nearly unchanged when reducing the length of the linkers. The ratio of the quantum dot areas for the two networks is $R = 1.83$, thus compared to confinement in a hexagonal box the expected scaling factor is somewhat larger than R_{exp}. This difference is consistent with the enlargement of the confining area produced by the attractive Co potential, that does not scale with the molecular length.

In conclusion, we have designed and fabricated room-temperature stable, self-assembled metal-organic networks that behave as arrays of coupled quantum dots. Our analysis points out that the 3-fold coordination of Co centers to CN groups alters the scattering characteristics of the Co atoms appreciably while those of the molecules remain essentially unchanged. The robustness of the metal-organic binding motif against a variation of the organic linker allows to control the confinement geometry and accordingly the electronic level alignment. A further functionalization of the molecules can provide an additional parameter to tailor the system. Thus, we introduced a versatile method to tune the interface electronic properties by employing an easy-to-control supramolecular protocol.

This work has been supported by the ERC Advanced Grant MolArt, the TUM Institute of Advanced Studies, the Deutsche Forschungsgemeinschaft (BA 3395/2-1), the Spanish MICINN (MAT2007-66050), the EU (NMP4-SL-2008-213660-ENSEMBLE), the Basque Departamento de Educación, UPV/EHU (Grant No. IT-366-07), and the Spanish Ministerio de Ciencia e Innovación (Grant No. FIS2010-19609-C02-01).

---

* Electronic address: florian.klappenberger@ph.tum.de

[1] N. Memmel, Surf. Sci. Rep. **32**, 93 (1998).

[2] M. F. Crommie, C. P. Lutz, and D. M. Eigler, Science **262**, 218 (1993).

[3] J. T. Li, W. D. Schneider, R. Berndt, O. R. Bryant, and S. Crampin, Phys. Rev. Lett. **81**, 4464 (1998).

[4] J. T. Li, W. D. Schneider, R. Berndt, and S. Crampin, Phys. Rev. Lett. **80**, 3332 (1998).

[5] J. Kliewer, *et al.*, Science **288**, 1399 (2000).

[6] K. F. Braun, and K. H. Rieder, Phys. Rev. Lett. **88**, 096801 (2002).

[7] H. Jensen, J. Kröger, R. Berndt, and S. Crampin, Phys. Rev. B **71**, 155417 (2005).

[8] C. Tournier-Colletta, B. Kierren, Y. Fagot-Revurat, and D. Malterre, Phys. Rev. Lett. **104**, 016802 (2010).

[9] G. A. Fiete, and E. J. Heller, Rev. Mod. Phys. **75**, 933 (2003).

[10] P. M. Echenique, *et al.*, Surf. Sci. Rep. **52**, 219 (2004).

[11] J. Kröger, *et al.*, Prog. Surf. Sci. **80**, 26 (2005).

[12] S. Crampin, H. Jensen, J. Kröger, L. Limot, and R. Berndt, Phys. Rev. B **72**, 035443 (2005).

[13] H. C. Manoharan, C. P. Lutz, and D. M. Eigler, Nature **403**, 512 (2000).

[14] J. Kliewer, R. Berndt, and S. Crampin, Phys. Rev. Lett. **85**, 4936 (2000).

[15] C. R. Moon, L. S. Mattos, B. K. Foster, G. Zeltzer, and H. C. Manoharan, Nat. Nanotechnol. **4**, 167 (2009).

[16] L. Gross, *et al.*, Phys. Rev. Lett. **93**, 056103 (2004).

[17] J. V. Barth, Annu. Rev. Phys. Chem. **58**, 375 (2007).

[18] Y. Pennec, *et al.*, Nat. Nanotechnol. **2**, 99 (2007).

[19] F. Klappenberger, *et al.*, Nano Lett. **9**, 3509 (2009).

[20] J. Lobo-Checa, *et al.*, Science **325**, 300 (2009).

[21] U. Schlickum, *et al.*, Nano Lett. **7**, 3813 (2007).

[22] D. Kühne, *et al.*, J. Am. Chem. Soc. **131**, 3881 (2009).

[23] F. J. Garcia de Abajo, J. Cordon, M. Corso, F. Schiller, and J. E. Ortega, Nanoscale **2**, 717 (2010).

[24] S. I. Bozhevolnyi, J. Erland, K. Leosson, P. M. W. Skovgaard, and J. M. Hvam, Phys. Rev. Lett. **86**, 3008 (2001).

[25] D. Kühne, *et al.*, J. Phys. Chem. C **113**, 17851 (2009).

[26] S. Clair, Ph.D. thesis, Ecole Polytechnique Fédérale de Lausanne (2004).

[27] J. T. Li, W. D. Schneider, and R. Berndt, Phys. Rev. B **56**, 7656 (1997).

[28] L. Bürgi, O. Jeandupeux, A. Hirstein, H. Brune, and K. Kern, Phys. Rev. Lett. **81**, 5370 (1998).

[29] J. Li, W. D. Schneider, S. Crampin, and R. Berndt, Surf. Sci. **422**, 95 (1999).

[30] V. Myroshnychenko, *et al.*, Adv. Mater. **20**, 4288 (2008).

[31] M. A. Schneider, *et al.*, Appl. Phys. A-Mater. Sci. Process. **80**, 937 (2005).

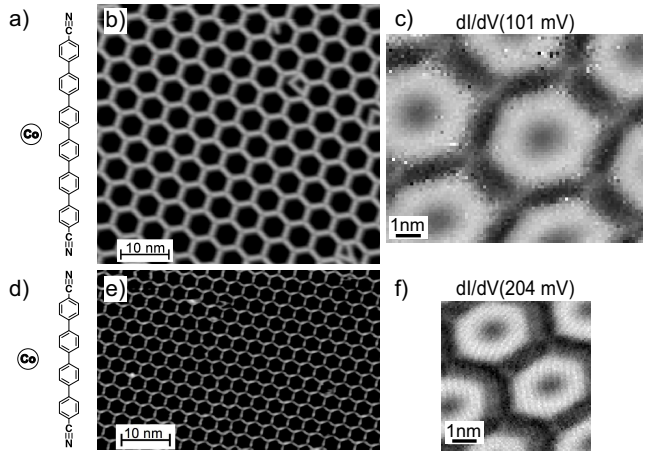

FIG. 1: (a) The self-assembly of NC-Ph_6-CN and Co produces (b) a crystal-quality metal-organic 2D network with honeycomb-shaped pores (STM image, $V_B = 1$ V, $I_T = 0.1$ nA). (c) The experimental dI/dV map (STS, $V_B = 101$ mV) shows a uniform electron standing wave pattern in all pores qualifying them as quantum dots. The lateral confinement dimensions are tunable by choice of the length of the molecules. (d) The shorter linking species creates (e) a network of the same symmetry, but with a smaller unit cell (STM image, $V_B = 0.8$ V, $I_T = 0.1$ nA) resulting (f) in the same electron wave pattern as in (c) but at an increased v_B.

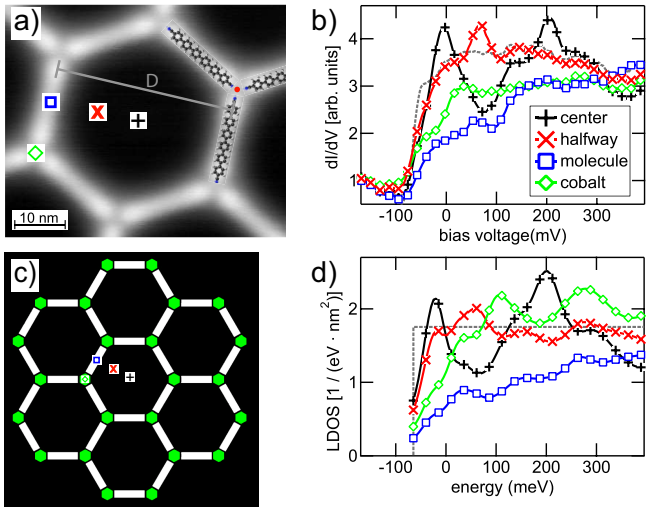

FIG. 2: (color online). (a) Topograph of a single quantum dot. The symbols depict the positions at which the dI/dV spectra of (b) were taken. D is the distance between parallel sides. (b) The experimental dI/dV spectra (symbols) demonstrate a strong position dependent modulation of the nearly constant DOS of the pristine surface (dashed line). (c) The 2D potential model with black, white and green areas corresponding to potential values of $V_0 = 0$ meV, $V_{\mathrm{mol}} = 500$ meV, and $V_{\mathrm{Co}} = -50$ meV. (d) The spectra calculated with the BEM.

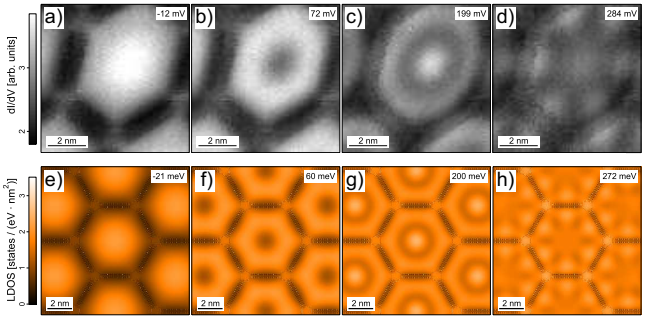

FIG. 3: (color online). (a)-(d) Measured dI/dV maps of a hexagonal quantum dot at indicated bias. (e)-(h) The electron wave patterns obtained with the BEM for the model potential of Fig. 2(c) reproduce well the characteristics of the experimental maps.

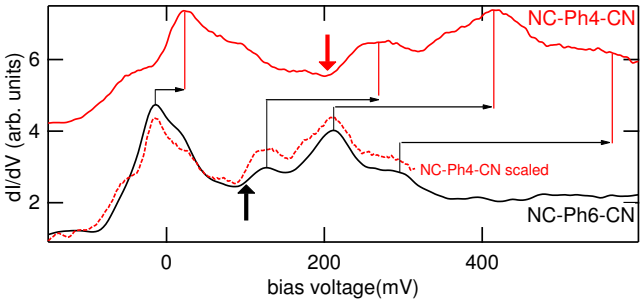

FIG. 4: (color online). The c-spectrum for cavities made with NC-Ph_6-CN linkers (black) and with NC-Ph_4-CN linkers (red). The four local maxima are present in both spectra but are upshifted for the shorter molecules as clearly demonstrated by the scaled version (red, dashed) of the NC-Ph_4-CN spectrum for which the bias values were scaled by the ratio of the confining areas of the two cases (for details see SI). The bold arrows signal the energies of the maps presented in Fig. 1c and f.